EurJIC
European Journal of Inorganic Chemistry

Research Article
doi.org/10.1002/ejic.202300300

Chemistry Europe
European Chemical Societies Publishing

www.eurjic.org

Special Collection

Immobilization of Iridium Triazolylidene Complexes into Polymer Scaffolds and Their Application in Water Oxidation

Pascal Knörr,[a] Nicolas Lentz,[a] and Martin Albrecht*[a]

A triazolylidene iridium complex was postmodified with simple methods to introduce two alcohol groups in the triazolylidene backbone. The reaction of this difunctionalized iridium triazolylidene unit with terephthalic acid chloride allowed for integrating these iridium complexes into a polymeric assembly. Both the monomeric complexes as well as the polymerized systems showed activity in water oxidation driven by cerium ammonium nitrate as a chemical oxidant with comparable catalytic performance. Post-reaction analysis of the aqueous reaction solution by ICP MS showed a partial loss of iridium from the polymer into the aqueous phase under catalytic conditions, indicating a need for more robust polymer supports for this type of application.

Introduction

The facile storage of renewably produced energy is a key condition to reduce our dependence on fossil resources, and hence, the development of alternative fuels has attracted great interest in recent years.[1–4] In nature, photosynthesis allows plants to store solar energy in chemical bonds through the splitting of water and the formation of energy-rich ATP, which powers the fixation of CO_2 into carbohydrates. Even though the photosynthetic pathways are well understood, the complexity and sophistication of the involved systems prevent a direct translation into artificial devices.[5–9] To conceive artificial photosynthesis, therefore two distinct half reactions need to be managed, consisting of oxidation to provide electrons and protons, and reduction of a feedstock molecule to generate energy-dense fuels such as hydrogen, methanol, or formic acid.[10–13] The oxidative process has been focusing on water oxidation (WO) and is generally considered as the more difficult half-reaction and thus the limiting factor in developing efficient artificial photosynthesis.[14] The increase of WO performance requires suitable catalysts that lower the barriers of the electron transfer and O–O bond formation to enhance overall energy conversion efficiencies. Molecularly defined systems[15,16] based on iridium[17–31] and ruthenium[32–39] complexes have shown particular promise in this field[40–46] with remarkably high turnover frequencies (TOFs) and turnover numbers (TONs).[22,47] While these homogeneous systems stand out with well-defined active sites that allow the activity to be finely tailored, their commercial application is surmised to require electrochemical cells and heterogeneous catalytic systems to keep a close proximity of the catalyst to the electrode surface. Heterogeneization of molecular catalysts can address this aspect by anchoring well-defined complexes to a solid matrix.[48–50] This approach allows to preserve the tailored catalytical activity of the metal center, in contrast to heterogeneous systems with ill-defined active sites where only fractions of the used material are engaged in catalysis.[51]

Several strategies have been developed to heterogeneise homogeneous WO systems.[52–65] Common to these strategies is the importance of rational ligand design.[66,67] The ligands must feature suitable functionalities that allow linkage to either a support matrix or to form solids based on the catalyst itself, which creates a self-supported system.[68] We reasoned that a chelated iridium(III) triazolylidene complex provides a suitable starting point to generate a heterogeneized construct, as this complex family has shown good performance in WO when the carbene is supported by a chelating donor site.[69] Moreover, the triazole backbone of these carbenes is synthetically easy to access through methods that tolerate a wide range of functional groups,[70–74] thus offering opportunities to tailor the ligand both, for robust iridium binding, and for backbone functionalization.[75] Here we present an iridium NHC complex with a bi-functional ligand that allows for heterogeneizing the iridium-carbene synthon via integration into a polymer with simple techniques. Key for this methodology is the high robustness of the iridium-carbene bond,[76] which enables a series of postmodifications of the complex to form (NHC)iridium-containing polyethylene terephthalate (PET) -derived polyesters for WO catalysis.

[a] P. Knörr, N. Lentz, M. Albrecht
Department of Chemistry
Biochemistry & Pharmaceutical Sciences
University of Bern
Freiestrasse 3
3012 Bern (Switzerland)
E-mail: martin.albrecht@unibe.ch

Supporting information for this article is available on the WWW under https://doi.org/10.1002/ejic.202300300

Special Collection Part of the "NHC-Ligands in Organometallic Chemistry and Catalysis" Special Collection.

Research Article
doi.org/10.1002/ejic.202300300

Results and Discussion

Ligand synthesis started from commercially available methyl 4′-amino-[1,1′-biphenyl]-4-carboxylate which was transformed to the corresponding azide **1** by reaction with t-BuONO and $TMSN_3$ (Scheme 1).[77] Copper-catalyzed alkyne azide cycloaddition with commercial methyl 4-ethynylbenzoate yielded the triazole **2** in 53% overall yield. We used the copper carbene complex [(IPr)CuCl] (IPr=N,N′-di(2,6-diisopropylaryl)imidazol-2-ylidene) with 2,2-bipyridine added in situ to catalyze the cycloaddition as typical simple copper sources only gave marginal conversions of 10–20% compared to 60% with the NHC complex.[78] Methylation with trifluoromethanesulfonate gave the triazolium salt **3** as the ligand precursor. Iridium complex **4** was prepared via a well-established transmetallation procedure[79] with Ag_2O. To this end, ligand precursor **3**, NMe_4Cl and Ag_2O were stirred under exclusion of light to yield the Ag-carbene complex. The solution was then filtered onto a mixture of the iridium precursor $[IrCp^*Cl_2]_2$ and sodium acetate, the latter facilitating cyclometallation. Simple purification by silica column chromatography yielded complex **4** as a pure yellow solid in 68% yield. Complex formation was indicated in by a diagnostic HR-MS signal with $m/z = 754.2257$ (754.2257 calculated for [**4**-Cl]$^+$). In ^{1}H NMR spectroscopy successful coordination was inferred by the disappearance of the $C_{trz}H$ resonance at $\delta_H = 10.01$ as well as one of the aryl signals in agreement with cyclometallation. X-ray diffraction analysis of single crystals of **4**, grown by vapour diffusion of Et_2O into a CH_2Cl_2 solution of **4**, unambiguously confirmed the proposed structure (Scheme 1).

Due to the high robustness of the Ir–C_{trz} bond in chelated triazolylidene complexes,[76] a set of post-modifications of the distal ester groups of complex **4** was feasible without any detectable demetallation. Thus, the two methylester groups on either side of the triazolylidene ligand backbone were converted to hydroxyethylesters to introduce two free alcohol functionalities on the complex. Attempts to form the product by direct transesterificaiton from the methylester complex **4** were unsuccessful. Instead, the (bis)carboxylic acid complex **5** was therefore synthesized as an intermediate. To this end, both methylester functionalities were hydrolyzed with aqueous NaOH and extracted with CH_2Cl_2, which provided complex **5** in 85% yield. Successful reaction was indicated by a diagnostic m/z signal at 762.1701 (762.1716 calculated for [**5**-H]$^+$). In the ^{1}H NMR spectrum, the methylester resonances at $\delta_H = 4.00$ and 3.95 disappeared in agreement with ester hydrolysis. Single crystal X-ray diffraction further supported the loss of the methyl groups (Scheme 1). Complex **6** was subsequently prepared in a second post-modification step by a classic esterification reac-

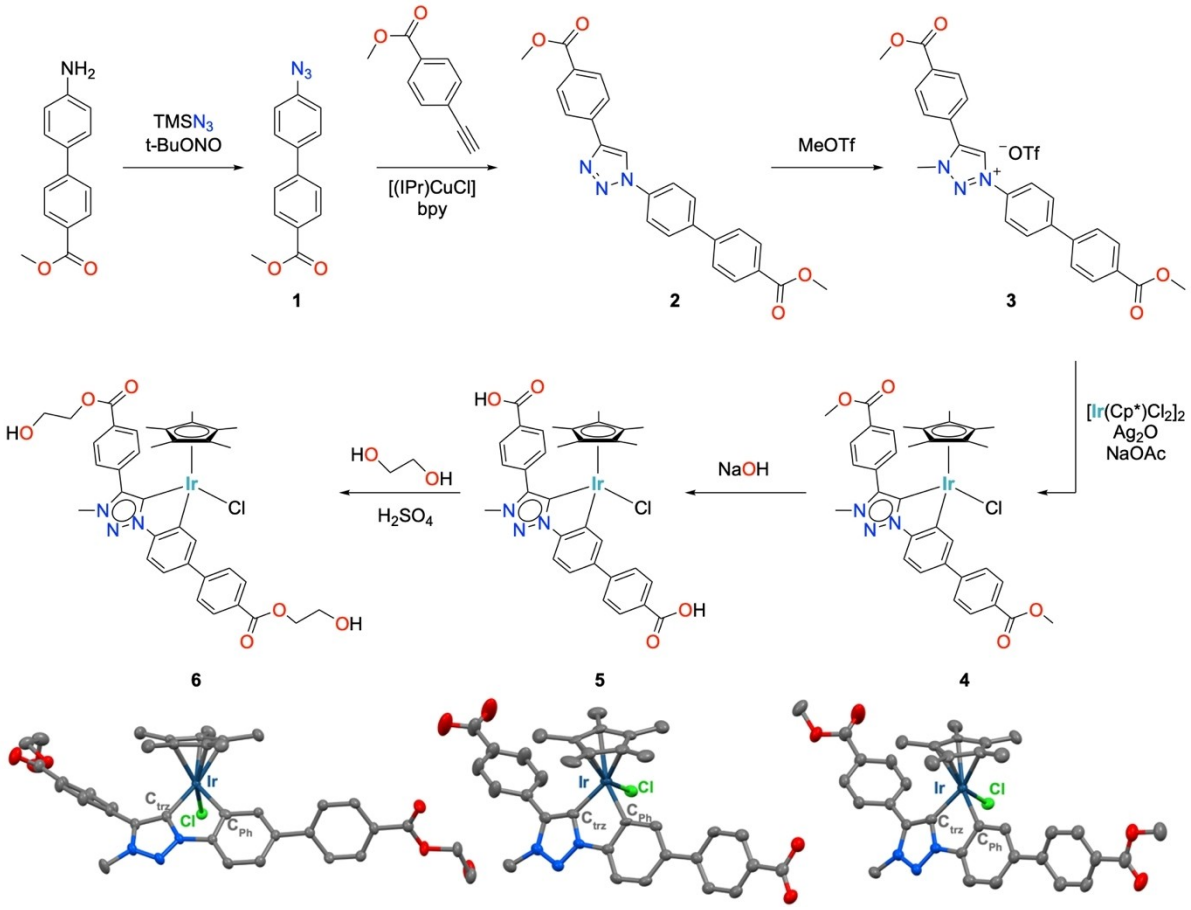

Scheme 1. Synthesis of ligand precursors **1**–**3** and iridium complexes **4**–**6**. Bottom: thermal ellipsoid plots of the molecular structures of complexes **4**–**6** (50% probability, hydrogen atoms and cocrystallized CH_2Cl_2 molecule in **6** omitted for clarity).

Research Article
doi.org/10.1002/ejic.202300300

Chemistry Europe
European Chemical Societies Publishing

tion involving the di(acid) iridium complex **5** and ethylene glycol as a solvent and reagent. Heating this mixture in the presence of catalytic amounts of H_2SO_4 followed by column chromatographic purification gave complex **6** as an analytically pure yellow solid in 60% yield. Successful modification was indicated by two multiplets in the ^{1}H NMR spectrum in the 4.58–4.41 and 4.02–3.91 ranges, consistent with the introduction of two ethylene glycol esters. Moreover, HR-MS revealed a m/z signal at 814.2468 (814.2437 calculated for [**6**-Cl]$^+$) and single crystal X-ray diffraction analysis showed the hydroxyethyl tether in the ligand backbone (Scheme 1).

Single crystal X-ray analysis of the complexes before and after post-modifications indicate that the Cp* iridium carbene core is unaffected by the reactions. All complexes in this series show the classic three-legged piano stool geometry. Both, the Ir–C_{ph} bond (2.060(8) Å) as well as the Ir–C_{trz} bond (2.025(15) Å) are identical within esds in complexes **4**–**6** (Table 1), demonstrating that the remote ligand modifications exert negligible electronic effects on the coordinated metal center. Likewise, the bond angles around iridium do not show any significant differences. Therefore, the remote transformations at the ligand backbone are expected to keep the catalytic activity unaltered with respect to the parent complex.

With complex **6** preliminary polymerization studies were carried out to test the stability of the iridium complex in presence of acyl chlorides. A CH_2Cl_2 solution of **6** and terephthaloyl chloride (1:1) was treated with NEt_3 and stirred for an hour at room temperature. The yellow solution was then washed with water and analyzed. ^{1}H NMR spectroscopy showed overall slightly broadened resonances and distinct changes around δ_H = 3.5–4.8, indicating reaction of the ethylenehydroxide groups with acyl chlorides. The aromatic resonances at δ_H = 7.0–8.3 did not shift significantly, suggesting that the iridium complex remained unaltered with persistent ligand coordination. From HR-MS analysis, the formation of oligomeric fragments was inferred from *m/z* signals, at 1793.4663 (1793.4680 calculated for the dimer **6**-C(O)–C_6H_4–C(O)-**6** as [M–Cl]$^+$). These results indicate that reaction of **6** with terephthaloyl chloride is feasible under mild conditions and does not lead to noticeable decomposition of the iridium complex.

Since a polymer consisting of just terephthate-bridged complex **6** would feature a very high iridium content, which may induce different WO mechanisms, the iridium loading of the polymer was lowered by introducing commercially available bis(2-hydroxyethyl)terephthalate as a co-monomer. This diol has the same functional groups as complex **6** and is therefore assumed to exert the same reactivity towards the terephthaloyl chloride linker. Sufficient dilution of complex **6** with this co-monomer should ensure that each complex forms an isolated mononuclear active catalytic site. Hence, a 1:9 molar mixture of iridium diol **6** and metal-free terephthalate co-monomer in CH_2Cl_2 was reacted with terephthaloyl chloride (10 moleq) in the presence of NEt_3 as a base (Scheme 2). The initial monomer suspension turned immediately to a clear yellow solution upon addition of NEt_3. After 30 s, the solution started to turn turbid, indicating formation of an insoluble fraction. Subsequently, the viscosity increased considerably to the point that magnetic stirring of the reaction mixture became ineffective, indicating the formation of an extensive polymer network. The solid product was filtered off and washed with acetone, water, CH_2Cl_2 and Et_2O to extract all residual monomer and co-monomer, as well as potentially soluble small oligomeric fractions. The product was then dried to yield the polymeric system **7** as a yellow solid. The polymer is insoluble in solvents such as $CDCl_3$, acetone, MeOH, DMSO, or CH_3CN, that is, solvents which dissolve the iridium monomer complex **6** well. Notably, polymer **7** is slightly soluble in a 1:1 mixture of hexafluoroisopropanol (HFIP) and $CDCl_3$, analogous to polyethylene terephthalate.[80] The ^{1}H NMR spectrum of **7** in this solvent mixture shows distinct differences to complex **6** (Figure S11). In particular, intense signals in the aromatic region around δ_H = 7.9–8.3 correlate well

Table 1. Selected bond lengths [Å] and angles [deg] of complexes **4**–**6**.

	4	5	6
Ir–C_{trz}	2.025(4)	2.037(4)	2.015(6)
Ir–C_{ph}	2.064(4)	2.061(3)	2.057(5)
Ir–Cl	2.419(1)	2.407(1)	2.437(1)
C_{trz}–Ir–C_{ph}	78.5(1)	78.4(1)	77.4(2)
C_{ph}–Ir–Cl	89.4(1)	89.5(1)	89.9(2)
Cl–Ir–C_{trz}	87.1(1)	87.6(1)	89.0(2)

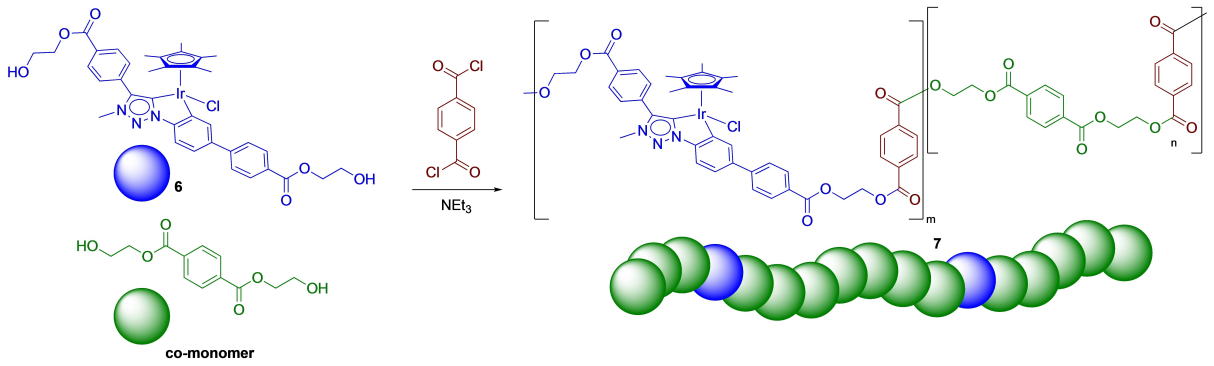

Scheme 2. Polymerization of iridium complex **6** with bis(2-hydroxyethyl)terephthalate as co-monomer, and terephthaloyl chloride as linker to give iridium-containing polymer **7**. Reaction conditions: **6** (30.0 mg, 35.3 µmol), terephthaloyl chloride (78.9 mg, 389 µmol), bis(2-hydroxyethyl)terephthalate (89.8 mg, 353 µmol) and NEt_3 (0.45 mL, 3.2 mmol) in CH_2Cl_2 (2.5 mL).

Research Article
doi.org/10.1002/ejic.202300300

with the aromatic terephthalate linker units. Furthermore, heating the polymer as a DMSO suspension to 100 °C led to considerable swelling and broad aromatic ^{1}H NMR signals at $\delta_H = 7.70–8.10$ together with a broad resonance at $\delta_H = 4.6$ (Figure S12), in agreement with extensive polyethylene terephthalate interlinkage. The broadness of the signals may be rationalized by the low solubility and potential coiling of the polymer. Inductively coupled plasma mass spectrometry (ICP-MS) yielded an iridium loading of the polymer of 34 μg_{Ir}/$mg_{polymer}$, which equals to 85 % of the theoretical loading based on the reaction stoichiometry. Further polymer analysis, for example to identify the polydispersity, was prevented by the very low solubility of polymeric **7**, though the excessive washing with solvents that solubilize the monomeric components indicates that **7** is composed of polymeric material only.

The single-site molecular complexes **4** and **6**, and the polymerized variant **7** were tested as WO catalysts. WO catalysis with iridium triazolylidene complexes has been established previously and these complexes are usually stable and active for a long time,[69] making this reaction well-suited for studying recyclability of the polymer. Cerium ammonium nitrate (CAN) was used a sacrificial one-electron oxidant, which is unable to catalyze the formation of dioxygen on its own.[81] As complex **4** is essentially insoluble in H_2O, a stock solution in CH_3CN was evaporated before adding H_2O and CAN. Catalytic runs were performed with a 1 : 8,000 Ir/CAN ratio and conversion was measured via the volume of the evolved gas using a BlueVcount volumetric gas counter (Figure 1). After CAN addition (as a solution in 1 M HNO_3), the complex rapidly solubilizes, and after an induction time of about 20 min gas evolution started. The induction time has been attributed predominantly to the insolubility of **4** and to the activation of the catalyst precursor, as often observed with iridium WO catalysts.[69] This activation is well-documented for Ir(Cp*)-based systems and involves replacement of the ancillary chloride ligand, oxidation of the iridium(III) center, and (partial) oxidation of the Cp* moiety.[82–85] Ancillary chelating ligands are usually retained during this process.[84] With complex **4** up to 1,200 turnovers were reached before the reaction stopped, which equals to about 60 % of the theoretical limit for oxygen production (2,000 TON, 22.7 mL O_2). A maximal turnover frequency $TOF_{max} = 900\ h^{-1}$ was noted after the induction period, which is within the range of many other homogeneous Ir(Cp*) catalysts for this reaction, yet well below some of the most active systems currently known (TOF_{max} 6,000–18,000 h^{-1}).[86,87]

Complex **6** was assessed under similar conditions and in addition also in the presence of 19 eq of bis(2-hydroxyethyl)terephthalate to mimic the presence of polymeric linkers present in **7**. The catalytic performance of **6** was similar to that of **4** ($TOF_{max} = 1{,}400\ h^{-1}$), yet it diminished drastically in the presence of terephthalate ($TOF_{max} = 100\ h^{-1}$), likely because oxidation of the alcohol sites is a competitive process to WO. Also the TONs of complex **6** (TON = 1,500) compare well to **4** only in the absence of added monomer. At the end of the catalytic run, the reaction solution was filtered over a glass fiber filter and the filter washed with 1 M HNO_3. When analyzed by ICP-MS, the filtrate was comprised of 79 ± 9 µg iridium. This amount equals to ca 80 % of the initially added iridium and indicates that this quantity was present either as homogeneous complex or as soluble decomposition products. The residual 20 % iridium may either be unactivated and hence insoluble complex **6**, a poorly soluble catalyst resting state, or insoluble iridium oxide from complex decomposition. When performing a catalyst recycling experiment by using the residue from the reaction flask and filter, some activity persisted. Gas evolution was considerably slower, which was expected as the iridium

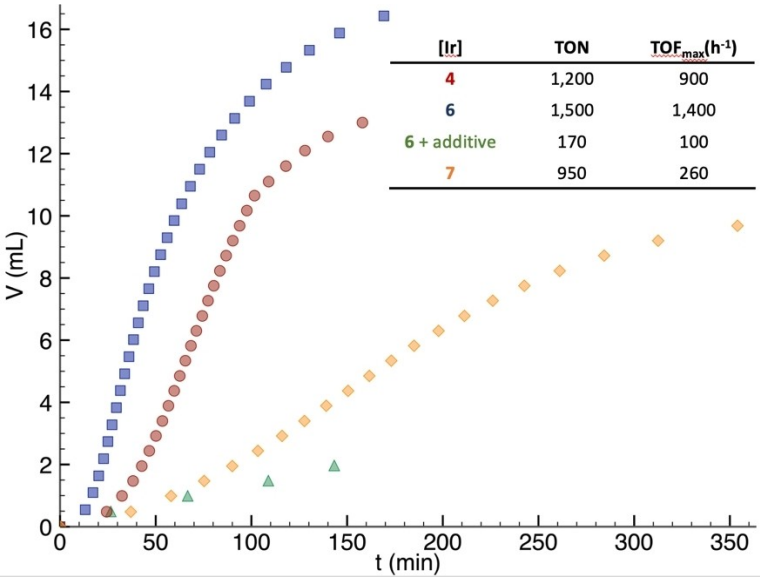

[Ir]	TON	TOF_{max} (h^{-1})
4	1,200	900
6	1,500	1,400
6 + additive	170	100
7	950	260

Figure 1. Time-dependent gas evolution profiles for WO with Ir complexes **4** (red circles), **6** (blue squares), **6** in the presence of bis(2-hydroxyethyl)terephthalate (19 eq, 9.5 µmol, green triangles), and with Ir-containing polymer **7** (yellow diamonds). Reaction conditions: 8,000 : 1 CAN/Ir ratio (0.4 M CAN in 1 M HNO_3 (10 mL), 50 µM [**Ir**] (8,000 : 1 CAN/Ir ratio; max O_2 volume = 22.7 mL); TOF_{max} calculated at the highest oxygen evolution rate and assuming full solubility of the iridium sites.

Research Article
doi.org/10.1002/ejic.202300300

loading was significantly decreased (Figure 2). However, taking the actual 20% loading into account, the TOF_{max} was estimated to be about equal to the first run, and TON_{max} remained in the same order of magnitude (ca. 1000). While the exact values need to be used with caution as the quantity of iridium was very small and errors accordingly are very large, they suggest that either the reused iridium was still bound to the chelating ligand, with limited solubility in the resting state, or that complex degradation to iridium oxide constitutes the active heterogeneous catalyst. Filtration of the solution after the second run followed by ICP-MS analysis indicated that all iridium was solubilized, which does not support the formation of a heterogeneous iridium oxide layer as active catalyst. In agreement with such a model, a catalytic run starting with only 80% catalyst loading (40 μM instead of 50 μM) afforded identical turnover frequencies and slightly lower TONs (ca. 720). Notably, a second recyclying experiment as described above did not show any more gas production and no residual catalytic activity, indicating that at these concentrations, all catalyst is in solution.

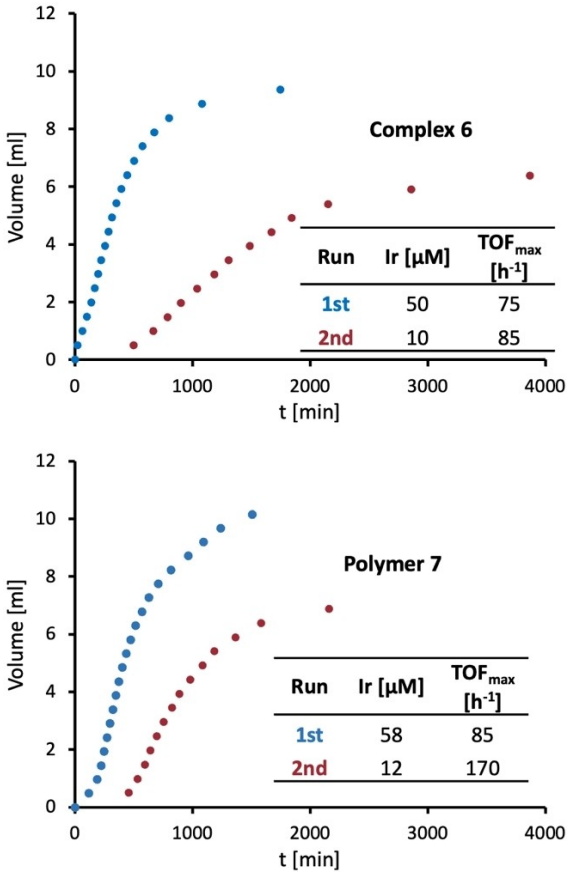

Figure 2. WO catalysis with complex **6** and polymer **7** before and after filtration. For both catalyst precursors time dependent gas evolution profiles are shown corresponding to inital runs (1st) and after recycling the catalyst (2nd). Reaction conditions: 0.4 M CAN in 1 M HNO_3 (10 mL), 50 μM [**Ir**] (8,000:1 CAN/Ir ratio, max O_2 volume = 22.7 mL). After initial runs, solids were filtered off, rinsed with 1 M HNO_3, and reused for the indicated 2nd runs; TOF_{max} calculated at the highest oxygen evolution rate and assuming full solubility of the iridium sites.

Under similar conditions, polymer **7** showed a 5-fold decrease in performance to the molecular complex **6** with $TOF_{max} \approx 260\ h^{-1}$, and the induction time was twice as long. Once gas evolution stopped, the polymer was reused according to the same procedure as applied for complex **6**, that is, separation of the solids from the solution via a glass fiber filter. ICP-MS analysis of the solution showed a total of 86 ± 10 μg iridum in solution (ca. 80% of initial loading). The concentration of iridium in solution is comparable to complex **6** and suggests that only about 20% residual iridium after the first cycle. Performing a second run with this 20% retained iridium fraction from the polymer showed increased catalytic activity ($TOF_{max} \approx 170\ h^{-1}$; Figure 2), which may speculatively be attributed to partial degradation of the polymer to smaller oligomeric fractions. ICP-MS of the filtrate after this second run revealed close to 25% of initial iridium loading, indicating that all residual iridium was solubilized at this stage. This behavior of polymer **7** is essentially identical to that of the monomeric molecular complex **6**, suggesting that (i) embedding of the catalytically active site into the polyethylene terephthalate structure has no negative impact on catalyst performance, and (ii) that the catalytically active species may be similar or identical both in initial runs and after recycling in the second runs. This similarity and the solubilization of the polymer-immobilized iridium within two runs further indicates that the polymeric backbone is unstable under catalytic conditions. Alternatively, catalyst activation may involve loss of the *N,C*-bidentate chelating phenyl-triazolylidene ligand from the iridium center and leaching of iridium into the solution. Reactions at lower iridium concentrations (*vide supra*) support, however, the former pathway and are not consistent with ligand loss.

The polymer-supported iridium catalyst therefore appears to depolymerize and release oligomeric or even monomeric iridium complexes similar to **6** into the reaction mixture. This reactivity may be due to the relatively harsh conditions when WO is driven by CAN as the sacrificial oxidant. Indeed, exposure of the polymer system **7** to acidic conditions (1 M HNO_3, pH = 0) as typical for CAN-mediated WO catalysis indicates the gradual formation of bis(2-hydroxyethyl)terephthalate according to ^{1}H NMR spectroscopic monitoring (Figure S14). This release, together with the catalytically inhibiting effect of the terephthalate on WO therefore rationalizes both, the lower activity of the **7** compared to the molecular systems **4** and **6**, as well as the loss of iridium, presumably as iridium complex **5** upon PET backbone acidolysis. Iridium-containing polymer **7** should therefore be applied under milder reaction conditions. For example, WO with different driving forces such as $NaIO_4$ as sacrificial oxidant, or electrocatalytic WO may change the activity,[69] and thus highlight the potential of this simple heterogeneization methodology.

Conclusions

We have demonstrated that the synthetic versatility of triazole-derived "click"-carbenes offers straightforward methodologies

Research Article
doi.org/10.1002/ejic.202300300

to embed triazolylidene metal complexes into polymeric structures as a viable strategy for the immobilization of homogeneous catalysts. The extraordinary stability of triazolylidene iridium complexes allowed for a range of post-functionalizations of the complexes, including base-mediated hydrolysis and acid-catalyzed esterification reactions to access iridium-carbene systems integrated into polyester materials. These iridium polymers catalyze the CAN-driven water oxidation, though recycling experiments show identical behavior as monomeric analogues, which suggests a breakdown of the polymeric structure under catalytic conditions. Thus, while the iridium binding site appears to be robust, the polymeric support is not. Based on these results, it may be beneficial to embed the active sites into more robust polymer structures, or to perform the water oxidation in an electrocatalytic set-up for remediating such polymer breakdown and for improving the recyclability of the polymeric iridium system.

Experimental Section

All reagents were commercially available and used as received unless specified. NMR spectra were recorded at 25 °C on Bruker spectrometers operating at 300 or 400 MHz (^{1}H NMR) and 75 or 100 MHz (^{13}C{^{1}H} NMR), respectively. Chemical shifts (δ in ppm, coupling constants *J* in Hz) were referenced to residual solvent signals (^{1}H,^{13}C). Assignments are based on homo- and hetero nuclear shift correlation spectroscopy. High resolution mass spectrometry was carried out by the DCBP mass spectrometry group at the University of Bern with with a Thermo Scientific LTQ Orbitrap XL (ESI-TOF). Elemental analyses were performed on a Thermo Scientific Flash 2000 CHNS-O elemental analyzer by the DCBP Microanalytic Laboratory. ICP measurements were carried out by the group of Prof. Dr. Peter Broekmann at the university of Bern on an Perkin Elmer NexION 2000.

Synthesis of azide 1: Methyl-4′-amino-(1,1′-biphenyl)-4-carboxylate (800.00 mg, 3.52 mmol) was suspended in CH_3CN (30 mL) and cooled to 0 °C. t-Butyl nitrite (545.0 mg, 5.28 mmol) and subsequently azidotrimethylsilane (487.0 mg, 4.22 mmol) were added dropwise and the mixture was stirred for 24 h at r.t. All volatiles were removed under reduced pressure. The resulting solid was dissolved in ethyl acetate (100 mL) and washed with water (2×100 mL). The organic phase was dried over Na_2SO_4 and all volatiles were removed under reduced pressure yielding **1** as a light brown solid (813 mg, 91 %). ^{1}H NMR (400 MHz, $CDCl_3$) δ 8.20–8.06 (m, 2H, CH_{Ph}), 7.66–7.58 (m, 4H, CH_{Ph}), 7.16–7.08 (m, 2H, CH_{Ph}), 3.94 (s, 3H, CH_3). ^{13}C{^{1}H} NMR (101 MHz, $CDCl_3$) δ 167.05 ($COOCH_3$), 144.65, 140.29, 136.86, 130.36, 129.15, 128.78, 126.87, 119.71 (8×C_{Ph}H, 4×C_{Ph}), 52.29 (CH_3). HR-MS (m/z): Calculated for $[M+H]^+$ = 254.0924; found: 254.0922.

Synthesis of triazole 2: Compound **1** (100 mg, 0.40 mmol), methyl-4-ethynylbenzoate (63 mg, 0.40 mmol) 2,2-bipyridine (4 mg, 0.02 mmol) and [(IPr)CuCl] (10 mg, 0.02 mmol) were dried under vacuum and suspended in dry CH_3CN (10 mL). The mixture was stirred at room temperature for 20 h. All solids were filtered of and washed with CH_3CN (10 mL) and CH_2Cl_2 (10 mL). The solids were dried under vacuum yielding triazole **2** as a light brown solid (100 mg, 61 %). ^{1}H NMR (400 MHz, $CDCl_3$) δ 8.33 (s, 1H, H_{trz}), 8.21–7.53 (m, 12H, H_{Ph}), 3.96 (s, 3H, OCH_3), 3.96 (s, 3H, OCH_3). HR-MS (m/z): Calculated for $[M+H]^+$ = 414.1448; found: 414.1439.

Synthesis of triazolium salt 3: Triazole **2** (100 mg, 0.24 mmol) was placed in a microwave vial and suspended in CH_2Cl_2 (6 mL). MeOTf (30 μL, 0.27 mmol) was added. The mixture was heated to 80 °C and stirred for 1.5 h. MeOH (1 mL) was added and the mixture was stirred for 1 h at room temperature. The mixture was concentrated under reduced pressure. Et_2O was then added until the product precipitated, yielding compound **3** (130 mg, 93 %) as a white solid. ^{1}H NMR (400 MHz, DMSO-d_6) δ 10.01 (s, 1H, C_{trz}H), 8.38–7.94 (m, 12H, C_{Ph}H), 4.48 (s, 3H, NCH_3), 3.94 (s, 3H, OCH_3), 3.90 (s, 3H, OCH_3). ^{13}C{^{1}H} NMR (101 MHz, DMSO) δ 165.93, 165.45 (2× COOMe), 142.45, 142.25, 141.99, 134.46, 132.25, 130.06, 129.98, 129.89, 129.52, 129.03, 127.89, 127.44, 126.84, 122.28, 121.87 (12×C_{Ph}, 2×C_{trz}, 1×C), 52.68, 52.32 (2×OCH_3), 38.5 (NCH_3). HR-MS (m/z): Calculated for $C_{25}H_{22}O_4N_3$[M-OTf]$^+$ = 428.1581; found: 428.1589. Anal. Calcd for $C_{25}H_{22}F_3N_3O_7S$ (577.53): C 54.07; H 3.84; N 7.28; S, 5.55 Found: C 54.36; H 3.91; N 7.17; S 5.53.

Synthesis of complex 4: Compound **2** (150.0 mg, 0.26 mmol), tetramethylammonium chloride (43.0 mg, 0.39 mmol) and Ag_2O (181.0 mg, 0.78 mmol) were placed in a schlenk flask and dried under vacuum. CH_2Cl_2 (10 mL) was added and the mixture was stirred for 48 h at r.t under exclusion of light. The mixture was filtered over Celite onto a mixture of $[Ir(Cp^*)Cl_2]_2$ (103.0 mg, 0.13 mmol) and sodium acetate (64.0 mg, 0.78 mmol) and stirred for 2 h. The mixture was filtered over Celite and all volatiles were removed under reduced pressure. The crude product was submitted to column chromatography (SiO_2; 2×CH_2Cl_2/MeOH 1000 : 4). All volatiles were removed under reduced pressure. The resulting solid was washed with pentane (3×10 mL), yielding complex **3** (140 mg, 68 %) as a yellow solid. ^{1}H NMR (400 MHz, $CDCl_3$) δ 8.26–8.20 (m, 2H, CH_{Ph}), 8.14–8.08 (m, 3H, CH_{Ph}), 7.98–7.91 (m, 2H, CH_{Ph}), 7.79–7.70 (m, 3H, CH_{Ph}), 7.31 (dd, *J* = 8.2, 1.9 Hz, 1H, CH_{Ph}), 4.14 (s, 3H, CH_3), 4.00 (s, 3H, CH_3), 3.95 (s, 3H, CH_3), 1.53 (s, 15H, Cp–CH_3). ^{13}C{^{1}H} NMR (101 MHz, $CDCl_3$) δ 167.36, 166.582 (2×COOH), 151.51 (C_{trz}Ir), 146.75, 145.54, 145.17, 143.07, 140.22 (5×C_q), 136.61, 132.68, 131.36, 130.86, 130.29, 130.08, 128.55, 127.41, 121.89, 112.54 (7×C_{Ph}, 2×C_q), 90.22 (C_q), 52.63, 52.19 (2×OCH_3), 37.50 (NCH_3), 9.49 (Cp–CH_3). Anal. Calcd for $C_{35}H_{35}ClIrN_3O_4$: C 53.26; H 4.47; N 5.32; Found: C 53.27; H 4.42; N 5.25. HR-MS (m/z): Calculated for $[M–Cl]^+$ = 754.2257; found: 754.2257.

Synthesis of complex 5: Complex **3** (130 mg, 0.16 mmol) was dissolved in acetone (100 mL). An NaOH solution (2 M in H_2O, 28 mL) was added and the mixture was stirred for 2 h at 35 °C. The mixture was concentrated under reduced pressure and washed with CH_2Cl_2 (1×50 mL). The aqueous phase was acidified with HCl (1 M) and extracted with EtOAc (100 mL). The organic phase was dried over Na_2SO_4 and evaporated to dryness. The crude product was washed twice with Et_2O yielding complex **4** (105 mg, 84 %) as a yellow solid. ^{1}H NMR (400 MHz, acetone-d_6) δ 8.29–8.23 (m, 2H, CH_{Ar}), 8.20–8.12 (m, 5H, CH_{Ar}), 7.91–7.85 (m, 2H, CH_{Ar}), 7.74 (m, 1H, CH_{Ar}), 7.40 (dd, *J* = 8.1, 2.0 Hz, 1H, CH_{Ar}), 4.34 (s, 3H, NCH_3), 1.54 (s, 15H, Cp–CH_3). ^{13}C{^{1}H} NMR (101 MHz, acetone-d_6) δ 167.58, 167.22, 152.25, 147.21, 146.45, 143.94, 140.12, 137.67, 133.87, 132.32, 131.88, 131.08, 130.77, 129.88, 127.93, 122.07, 114.11, 90.39, 38.21 (NCH_3), 9.46 (Cp–CH_3). HR-MS (m/z): Calculated for $[M+H]^+$ = 762.1716; found: 762.1701.

Synthesis of complex 6: Complex **5** (100.0 mg, 131.3 μmol) was placed in a Schlenk flask under nitrogen atmosphere. Ethylene glycol (11 mL, large excess) and H_2SO_4 (0.1 mL) were added and the mixture heated to 100 °C for 3 h. Completion of the reaction was indicated by full dissolution of previously suspended complex. The crude mixture was diluted with water (100 mL) and extracted with EtOAc (2×50 mL). The organic phase was washed once with aquaeous sat. Na_2CO_3 solution (20 mL), dried over $MgSO_4$ and evaporated to dryness under reduced pressure. The crude was submitted to gradient column chromatography (SiO_2; CH_2Cl_2/MeOH from 100:0 to 100 : 1.5). All volatiles were removed under reduced pressure and the resulting solid was dissolved in a minimal amount

Research Article
doi.org/10.1002/ejic.202300300

of CH_2Cl_2 and precipitated by addition of Et_2O. Precipitation was repeated from acetone solution. The solid was washed with Et_2O (3×20 mL) to yield complex **6** as a yellow powder (68 mg, 60%). ^{1}H NMR (400 MHz, CD_2Cl_2) δ 8.29–8.22 (m, 2H, CH_{ph}), 8.17–8.08 (m, 3H, CH_{ph}), 7.98–7.93 (m, 2H, CH_{ph}), 7.84–7.73 (m, 3H, CH_{ph}), 7.36 (dd, J= 8.2, 2.0 Hz, 1H, CH_{ph}), 4.58–4.41 (m, 4H, $COOCH_2$), 4.16 (s, 3H, trz-CH_3), 4.02–3.91 (m, 4H, CH_2OH), 2.07–1.97 (m, 2H, OH), 1.52 (s, 15H, Cp–CH_3). ^{13}C{^{1}H} NMR (101 MHz, CD_2Cl_2) δ 167.09, 166.55(2×COO), 151.97 (C_{trz}Ir), 146.95, 146.44, 143.32, 140.14, 138.05 (5×C_q), 136.92, 133.18, 131.48, 131.14, 130.49, 130.37, 127.66, 121.93, 114.04 (7×C_{Ph}, 2×C_q), 91.10 (C_q), 67.44, 67.08, 61.73, 61.58 (4×CH_2), 37.96 (NCH_3), 9.48 (Cp–CH_3). HR-MS (m/z): Calculated for $[M–Cl]^+$ = 814.2437; found: 814.2468. Anal. Calcd for $C_{37}H_{41}ClIrN_3O_6$: C 52.32; H 4.63; N 4.95; Found: C 52.33; H 4.42; N 4.62.

Synthesis of polymer 7: Under an atmosphere of N_2, complex **6** (30.0 mg, 35.3 μmol), terephthaloyl chloride (78.9 mg, 389 μmol), bis(2-hydroxyethyl)terephthalate (89.8 mg, 353 μmol) and anhydrous NEt_3 (0.45 mL, 3.2 mmol) were mixed in dry CH_2Cl_2 (2.5 mL), producing an intensely yellow solution. The solution was incubated at room temperature for 3 days (due to formation of solids, stirring stopped after several minutes). The formed solids were filtered off and washed with acetone, H_2O, CH_3CN CH_2Cl_2 and Et_2O. The product was dried under vacuum to yield a yellow waxy solid (121 mg, 71%). To determine the Ir content, polymer **7** was decomposed by heating a sample suspended in 60% HNO_3 at 80 °C for 2 days. After this treatment, the suspended solids lost their originally yellow color, and the mixture appeared as a colorless suspension containing white solids. The mixture was filtered over a glass filter, diluted with water and subjected to ICP-MS.

Typical catalytic procedure water oxidation: Complex **4** (395 μg, 0.5 μmol) was added to a 25 mL two neck round-bottom flask as a CH_3CN solution and evaporated to dryness. One neck was closed with a septum, the other connected to a BlueVCount volumetric gas counter. The gas counter automatically normalizes the measured volume for pressure, humidity and temperature. A CAN solution (0.4 M in 1 M aqueous HNO_3, 10 mL) was added and the solution was stirred at room temperature until gas formation ceased according to the BlueVCount measurements.

ICP-MS measurements after catalytic runs: The reaction mixture was filtered and the glassware and filter washed with HNO_3. The combined aqueous layers were weighted and submitted to ICP analysis which determined the iridium content in μg per g sample. Based on this data the total of leached iridium was calculated and compared to the initial catalytic loading to determine the amount of non-dissolved iridium.

Crystal-Structure Determination: Crystals of **4,5** and **6** were immersed in parabar oil, mounted at ambient conditions and transferred into the stream of nitrogen (173 K). The measurements of **4** and **5** were made on a *RIGAKU Synergy S* area-detector diffractometer[88] using mirror optics monochromated Cu *Kα* radiation (λ = 1.54184 Å). The measurement of **6** was made on a *Oxford Diffraction SuperNova* area-detector diffractometer[89] using mirror optics monochromated Mo *Kα* radiation (λ = 0.71073 Å) and Al filtered.[90] Data reduction was performed using the *CrysAlisPro*[89] program. The intensities were corrected for Lorentz and polarization effects, and an absorption correction based on the multi-scan method using SCALE3 ABSPACK in *CrysAlisPro*[89] was applied. The structures were solved by intrinsic phasing using *SHELXT*,[91] which revealed the positions of all non-hydrogen atoms. All atoms were refined anisotropically and H-atoms were assigned in geometrically calculated positions and refined using a riding model where each H-atom was assigned a fixed isotropic displacement parameter with a value equal to 1.2 Ueq of its parent atom (1.5 Ueq for methyl groups). For **4**, one methylester group is conformationally disordered about two sites. About 9% of the unit cell volume is filled by heavily disordered co-crystallized solvent molecules. For **5** the Cp* ligand is conformationally disordered about two sites. Its atomic displacement parameters were restrained using the SHELX SIMU and RIGU instructions. About 27% of the unit cell volume is filled by heavily disordered co-crystallized solvent molecules. Electron density of disordered solvent molecules was accounted for by the SQUEEZE procedure of PLATON.[92] Refinement of the structures were carried out on F^2 using full-matrix least-squares procedures, which minimized the function $\Sigma w(F_o^2–F_c^2)^2$. The weighting scheme was based on counting statistics and included a factor to downweight the intense reflections. All calculations were performed using the *SHELXL-2014/7*[93] program in OLEX2.[94] Further crystallographic details are compiled in Tables S3–5.

Deposition Number(s) 2258617 (**4**), 2258618 (**5**), and 2258619 (**6**) contain(s) the supplementary crystallographic data for this paper. These data are provided free of charge by the joint Cambridge Crystallographic Data Centre and Fachinformationszentrum Karlsruhe Access Structures service.

Acknowledgements

We thank Michael Garbe for technical assistance, the crystallography group of the DCBP for X-ray analysis, and the mass spectrometry group for MS-analysis. We acknowledge the Swiss National Science Foundation (grant 200020_2182663 and 200020_212863) for generous financial support. Open Access funding provided by Universität Bern.

Conflict of Interests

The authors declare no conflict of interest.

Data Availability Statement

The data that support the findings of this study are available in the supplementary material of this article.

Keywords: Iridium · Polymer support · Post-functionalization · Triazolylidene · Water oxidation catalysis

[1] C. Liu, F. Li, L.-P. Ma, H.-M. Cheng, *Adv. Mater.* **2010**, *22*, E28–E62.
[2] S. van Renssen, *Nat. Clim. Change* **2020**, *10*, 799–801.
[3] N. Armaroli, V. Balzani, *Energy Environ. Sci.* **2011**, *4*, 3193.
[4] N. Armaroli, V. Balzani, *Angew. Chem. Int. Ed.* **2007**, *46*, 52–66.
[5] S. Y. Reece, J. A. Hamel, K. Sung, T. D. Jarvi, A. J. Esswein, J. J. H. Pijpers, D. G. Nocera, *Science* **2011**, *334*, 645–648.
[6] S. Berardi, S. Drouet, L. Francàs, C. Gimbert-Suriñach, M. Guttentag, C. Richmond, T. Stoll, A. Llobet, *Chem. Soc. Rev.* **2014**, *43*, 7501–7519.
[7] J. J. Concepcion, R. L. House, J. M. Papanikolas, T. J. Meyer, *Proc. Natl. Acad. Sci. USA* **2012**, *109*, 15560–15564.
[8] D. Gust, T. A. Moore, A. L. Moore, *Acc. Chem. Res.* **2009**, *42*, 1890–1898.
[9] M. D. Kärkäs, E. V. Johnston, O. Verho, B. Åkermark, *Acc. Chem. Res.* **2014**, *47*, 100–111.
[10] C. Herrero, A. Quaranta, W. Leibl, A. W. Rutherford, A. Aukauloo, *Energy Environ. Sci.* **2011**, *4*, 2353.
[11] N. S. Lewis, D. G. Nocera, *Proc. Natl. Acad. Sci. USA* **2006**, *103*, 15729–15735.
[12] N. D. McDaniel, S. Bernhard, *Dalton Trans.* **2010**, *39*, 10021.

[13] C. G. Morales-Guio, L.-A. Stern, X. Hu, *Chem. Soc. Rev.* **2014**, *43*, 6555.
[14] J. K. Hurst, *Science* **2010**, *328*, 315–316.
[15] A. Llobet, Ed., *Molecular water oxidation catalysis: a key topic for new sustainable energy conversion schemes*, John Wiley & Sons, Inc, Chichester, West Sussex **2014**.
[16] N. Vereshchuk, M. Gil-Sepulcre, A. Ghaderian, J. Holub, C. Gimbert-Suriñach, A. Llobet, *Chem. Soc. Rev.* **2023**, *52*, 196–211.
[17] N. D. McDaniel, F. J. Coughlin, L. L. Tinker, S. Bernhard, *J. Am. Chem. Soc.* **2008**, *130*, 210–217.
[18] J. F. Hull, D. Balcells, J. D. Blakemore, C. D. Incarvito, O. Eisenstein, G. W. Brudvig, R. H. Crabtree, *J. Am. Chem. Soc.* **2009**, *131*, 8730–8731.
[19] J. D. Blakemore, N. D. Schley, D. Balcells, J. F. Hull, G. W. Olack, C. D. Incarvito, O. Eisenstein, G. W. Brudvig, R. H. Crabtree, *J. Am. Chem. Soc.* **2010**, *132*, 16017–16029.
[20] R. Lalrempuia, N. D. McDaniel, H. Müller-Bunz, S. Bernhard, M. Albrecht, *Angew. Chem. Int. Ed.* **2010**, *49*, 9765–9768.
[21] N. D. Schley, J. D. Blakemore, N. K. Subbaiyan, C. D. Incarvito, F. D'Souza, R. H. Crabtree, G. W. Brudvig, *J. Am. Chem. Soc.* **2011**, *133*, 10473–10481.
[22] Z. Codolà, J. M. S. Cardoso, B. Royo, M. Costas, J. Lloret-Fillol, *Chem. Eur. J.* **2013**, *19*, 7203–7213.
[23] O. Diaz-Morales, T. J. P. Hersbach, D. G. H. Hetterscheid, J. N. H. Reek, M. T. M. Koper, *J. Am. Chem. Soc.* **2014**, *136*, 10432–10439.
[24] A. Petronilho, J. A. Woods, S. Bernhard, M. Albrecht, *Eur. J. Inorg. Chem.* **2014**, *2014*, 708–714.
[25] M. Li, K. Takada, J. I. Goldsmith, S. Bernhard, *Inorg. Chem.* **2016**, *55*, 518–526.
[26] M. Navarro, M. Li, H. Müller-Bunz, S. Bernhard, M. Albrecht, *Chem. Eur. J.* **2016**, *22*, 6740–6745.
[27] G. Menendez Rodriguez, A. Bucci, R. Hutchinson, G. Bellachioma, C. Zuccaccia, S. Giovagnoli, H. Idriss, A. Macchioni, *ACS Energy Lett.* **2017**, *2*, 105–110.
[28] G. Menendez Rodriguez, G. Gatto, C. Zuccaccia, A. Macchioni, *ChemSusChem* **2017**, *10*, 4503–4509.
[29] R. Puerta-Oteo, M. V. Jiménez, J. J. Pérez-Torrente, *Catal. Sci. Technol.* **2019**, *9*, 1437–1450.
[30] Z. Mazloomi, J. Margalef, M. Gil-Sepulcre, N. Romero, M. Albrecht, A. Llobet, X. Sala, O. Pàmies, M. Diéguez, *Inorg. Chem.* **2020**, *59*, 12337–12347.
[31] G. Gatto, A. De Palo, A. C. Carrasco, A. M. Pizarro, S. Zacchini, G. Pampaloni, F. Marchetti, A. Macchioni, *Catal. Sci. Technol.* **2021**, *11*, 2885–2895.
[32] S. W. Gersten, G. J. Samuels, T. J. Meyer, *J. Am. Chem. Soc.* **1982**, *104*, 4029–4030.
[33] C. Sens, I. Romero, M. Rodríguez, A. Llobet, T. Parella, J. Benet-Buchholz, *J. Am. Chem. Soc.* **2004**, *126*, 7798–7799.
[34] R. Zong, R. P. Thummel, *J. Am. Chem. Soc.* **2005**, *127*, 12802–12803.
[35] S.-X. Guo, C.-Y. Lee, J. Zhang, A. M. Bond, Y. V. Geletii, C. L. Hill, *Inorg. Chem.* **2014**, *53*, 7561–7570.
[36] R. Matheu, L. Francàs, P. Chernev, M. Z. Ertem, V. Batista, M. Haumann, X. Sala, A. Llobet, *ACS Catal.* **2015**, *5*, 3422–3429.
[37] B. Limburg, E. Bouwman, S. Bonnet, *ACS Catal.* **2016**, *6*, 5273–5284.
[38] L. Tong, R. P. Thummel, *Chem. Sci.* **2016**, *7*, 6591–6603.
[39] T. Liu, S. Zhan, N. Shen, L. Wang, Z. Szabó, H. Yang, M. S. G. Ahlquist, L. Sun, *J. Am. Chem. Soc.* **2023**, jacs.3c03415.
[40] W. C. Ellis, N. D. McDaniel, S. Bernhard, T. J. Collins, *J. Am. Chem. Soc.* **2010**, *132*, 10990–10991.
[41] J. L. Fillol, Z. Codolà, I. Garcia-Bosch, L. Gómez, J. J. Pla, M. Costas, *Nat. Chem.* **2011**, *3*, 807–813.
[42] M. Wiechen, H.-M. Berends, P. Kurz, *Dalton Trans.* **2012**, *41*, 21–31.
[43] H. Lv, J. Song, Y. V. Geletii, J. W. Vickers, J. M. Sumliner, D. G. Musaev, P. Kögerler, P. F. Zhuk, J. Bacsa, G. Zhu, C. L. Hill, *J. Am. Chem. Soc.* **2014**, *136*, 9268–9271.
[44] F. Song, R. Moré, M. Schilling, G. Smolentsev, N. Azzaroli, T. Fox, S. Luber, G. R. Patzke, *J. Am. Chem. Soc.* **2017**, *139*, 14198–14208.
[45] M. Natali, I. Bazzan, S. Goberna-Ferrón, R. Al-Oweini, M. Ibrahim, B. S. Bassil, H. Dau, F. Scandola, J. R. Galán-Mascarós, U. Kortz, A. Sartorel, I. Zaharieva, M. Bonchio, *Green Chem.* **2017**, *19*, 2416–2426.
[46] M. Gil-Sepulcre, A. Llobet, *Nat. Catal.* **2022**, *5*, 79–82.
[47] L. Duan, F. Bozoglian, S. Mandal, B. Stewart, T. Privalov, A. Llobet, L. Sun, *Nat. Chem.* **2012**, *4*, 418–423.
[48] C. Wang, J.-L. Wang, W. Lin, *J. Am. Chem. Soc.* **2012**, *134*, 19895–19908.
[49] R. Matheu, I. A. Moreno-Hernandez, X. Sala, H. B. Gray, B. S. Brunschwig, A. Llobet, N. S. Lewis, *J. Am. Chem. Soc.* **2017**, *139*, 11345–11348.
[50] J. Odrobina, J. Scholz, A. Pannwitz, L. Francàs, S. Dechert, A. Llobet, C. Jooss, F. Meyer, *ACS Catal.* **2017**, *7*, 2116–2125.
[51] A. Macchioni, *Eur. J. Inorg. Chem.* **2019**, *2019*, 7–17.
[52] J. Mola, E. Mas-Marza, X. Sala, I. Romero, M. Rodríguez, C. Viñas, T. Parella, A. Llobet, *Angew. Chem. Int. Ed.* **2008**, *47*, 5830–5832.
[53] C. Wang, Z. Xie, K. E. deKrafft, W. Lin, *J. Am. Chem. Soc.* **2011**, *133*, 13445–13454.
[54] F. Li, B. Zhang, X. Li, Y. Jiang, L. Chen, Y. Li, L. Sun, *Angew. Chem. Int. Ed.* **2011**, *50*, 12276–12279.
[55] A. Savini, A. Bucci, M. Nocchetti, R. Vivani, H. Idriss, A. Macchioni, *ACS Catal.* **2015**, *5*, 264–271.
[56] S. W. Sheehan, J. M. Thomsen, U. Hintermair, R. H. Crabtree, G. W. Brudvig, C. A. Schmuttenmaer, *Nat. Commun.* **2015**, *6*, 6469.
[57] D. Wang, R. N. Sampaio, L. Troian-Gautier, S. L. Marquard, B. H. Farnum, B. D. Sherman, M. V. Sheridan, C. J. Dares, G. J. Meyer, T. J. Meyer, *J. Am. Chem. Soc.* **2019**, *141*, 7926–7933.
[58] D. Antón-García, J. Warnan, E. Reisner, *Chem. Sci.* **2020**, *11*, 12769–12776.
[59] X. Liang, S. Yang, J. Yang, W. Sun, X. Li, B. Ma, J. Huang, J. Zhang, L. Duan, Y. Ding, *Appl. Catal. B* **2021**, *291*, 120070.
[60] K. L. Materna, R. H. Crabtree, G. W. Brudvig, *Chem. Soc. Rev.* **2017**, *46*, 6099–6110.
[61] T. Keijer, T. Bouwens, J. Hessels, J. N. H. Reek, *Chem. Sci.* **2021**, *12*, 50–70.
[62] J. Li, C. A. Triana, W. Wan, D. P. Adiyeri Saseendran, Y. Zhao, S. E. Balaghi, S. Heidari, G. R. Patzke, *Chem. Soc. Rev.* **2021**, *50*, 2444–2485.
[63] C. Domestici, L. Tensi, F. Zaccaria, N. Kissimina, M. Valentini, R. D'Amato, F. Costantino, C. Zuccaccia, A. Macchioni, *Sci. Bull.* **2020**, *65*, 1614–1625.
[64] C. Domestici, L. Tensi, E. Boccalon, F. Zaccaria, F. Costantino, C. Zuccaccia, A. Macchioni, *Eur. J. Inorg. Chem.* **2021**, *2021*, 299–307.
[65] L. Tensi, A. V. Yakimov, C. Trotta, C. Domestici, J. De Jesus Silva, S. R. Docherty, C. Zuccaccia, C. Copéret, A. Macchioni, *Inorg. Chem.* **2022**, *61*, 10575–10586.
[66] F. Carson, E. Martínez-Castro, R. Marcos, G. G. Miera, K. Jansson, X. Zou, B. Martín-Matute, *Chem. Commun.* **2015**, *51*, 10864–10867.
[67] R. Zhong, A. C. Lindhorst, F. J. Groche, F. E. Kühn, *Chem. Rev.* **2017**, *117*, 1970–2058.
[68] D. Wang, S. L. Marquard, L. Troian-Gautier, M. V. Sheridan, B. D. Sherman, Y. Wang, M. S. Eberhart, B. H. Farnum, C. J. Dares, T. J. Meyer, *J. Am. Chem. Soc.* **2018**, *140*, 719–726.
[69] M. Olivares, C. J. M. van der Ham, V. Mdluli, M. Schmidtendorf, H. Müller-Bunz, T. W. G. M. Verhoeven, M. Li, J. W. (Hans) Niemantsverdriet, D. G. H. Hetterscheid, S. Bernhard, M. Albrecht, *Eur. J. Inorg. Chem.* **2020**, *2020*, 801–812.
[70] H. C. Kolb, M. G. Finn, K. B. Sharpless, *Angew. Chem. Int. Ed.* **2001**, *40*, 2004–2021.
[71] V. V. Rostovtsev, L. G. Green, V. V. Fokin, K. B. Sharpless, *Angew. Chem. Int. Ed.* **2002**, *41*, 2596–2599.
[72] C. W. Tornøe, C. Christensen, M. Meldal, *J. Org. Chem.* **2002**, *67*, 3057–3064.
[73] J. A. Prescher, D. H. Dube, C. R. Bertozzi, *Nature* **2004**, *430*, 873–877.
[74] B. T. Worrell, J. A. Malik, V. V. Fokin, *Science* **2013**, *340*, 457–460.
[75] Á. Vivancos, C. Segarra, M. Albrecht, *Chem. Rev.* **2018**, *118*, 9493–9586.
[76] A. Petronilho, J. A. Woods, H. Mueller-Bunz, S. Bernhard, M. Albrecht, *Chem. Eur. J.* **2014**, *20*, 15775–15784.
[77] F. Kloss, U. Köhn, B. O. Jahn, M. D. Hager, H. Görls, U. S. Schubert, *Chem. Asian J.* **2011**, *6*, 2816–2824.
[78] M.-L. Teyssot, L. Nauton, J.-L. Canet, F. Cisnetti, A. Chevry, A. Gautier, *Eur. J. Org. Chem.* **2010**, *2010*, 3507–03515.
[79] K. F. Donnelly, R. Lalrempuia, H. Müller-Bunz, M. Albrecht, *Organometallics* **2012**, *31*, 8414–8419.
[80] S. Farah, T. Tsach, A. Bentolila, A. J. Domb, *Talanta* **2014**, *123*, 54–62.
[81] A. R. Parent, R. H. Crabtree, G. W. Brudvig, *Chem. Soc. Rev.* **2013**, *42*, 2247–2252.
[82] A. Savini, P. Belanzoni, G. Bellachioma, C. Zuccaccia, D. Zuccaccia, A. Macchioni, *Green Chem.* **2011**, *13*, 3360.
[83] C. Zuccaccia, G. Bellachioma, O. Bortolini, A. Bucci, A. Savini, A. Macchioni, *Chem. Eur. J.* **2014**, *20*, 3446–3456.
[84] J. M. Thomsen, D. L. Huang, R. H. Crabtree, G. W. Brudvig, *Dalton Trans.* **2015**, *44*, 12452–12472.
[85] G. Hu, J. L. Troiano, U. T. Tayvah, L. S. Sharninghausen, S. B. Sinha, D. Y. Shopov, B. Q. Mercado, R. H. Crabtree, G. W. Brudvig, *Inorg. Chem.* **2021**, *60*, 14349–14356.
[86] A. Bucci, A. Savini, L. Rocchigiani, C. Zuccaccia, S. Rizzato, A. Albinati, A. Llobet, A. Macchioni, *Organometallics* **2012**, *31*, 8071–8074.
[87] I. Corbucci, A. Petronilho, H. Müller-Bunz, L. Rocchigiani, M. Albrecht, A. Macchioni, *ACS Catal.* **2015**, *5*, 2714–2718.

Research Article
doi.org/10.1002/ejic.202300300

[88] Oxford Diffraction, *CrysAlisPro, Version 1.171.40.37a*, Oxford Diffraction Ltd., Yarnton, Oxfordshire, UK **2018**.
[89] Oxford Diffraction, *CrysAlisPro, Version 1.171.38.41*, Oxford Diffraction Ltd., Yarnton, Oxfordshire, UK **2018**.
[90] P. Macchi, H.-B. Bürgi, A. S. Chimpri, J. Hauser, Z. Gál, *J. Appl. Crystallogr.* **2011**, *44*, 763–771.
[91] G. M. Sheldrick, *Acta Crystallogr. Sect. A* **2015**, *71*, 3–8.
[92] A. L. Spek, *Acta Crystallogr. Sect. C* **2015**, *71*, 9–18.
[93] G. M. Sheldrick, *Acta Crystallogr. Sect. C* **2015**, *71*, 3–8.
[94] O. V. Dolomanov, L. J. Bourhis, R. J. Gildea, J. A. K. Howard, H. Puschmann, *J. Appl. Crystallogr.* **2009**, *42*, 339–341.

Manuscript received: May 22, 2023
Revised manuscript received: July 31, 2023
Accepted manuscript online: July 31, 2023
Version of record online: August 24, 2023